Phase Diagram of Interacting Composite Fermions in the Bilayer $\nu = 2/3$ Quantum Hall Effect

N. Kumada, D. Terasawa, Y. Shimoda, H. Azuhata, A. Sawada, and Z. F. Ezawa
Department of Physics, Tohoku University, Sendai 980-8578, Japan

K. Muraki, T. Saku, and Y. Hirayama
NTT Basic Research Laboratories, 3-1 Morinosato-Wakamiya, Atsugi, Kanagawa 243-0198, Japan
(Received 13 December 2001; published 23 August 2002)

We study the phase diagram of composite fermions (CFs) in the presence of spin and pseudospin degrees of freedom in the bilayer $\nu = 2/3$ quantum Hall (QH) state. Activation studies elucidate the existence of three different QH states with two different types of hysteresis in the magnetotransport. While a noninteracting CF model provides a qualitative account of the phase diagram, the observed renormalization of tunneling gap and a non-QH state at high densities are not explained in the noninteracting CF model, and are suggested to be manifestations of interactions between CFs.

DOI: 10.1103/PhysRevLett.89.116802 PACS numbers: 73.43.Nq, 71.10.Pm, 73.21.Fg

The fractional quantum Hall effect (FQHE) is intuitively understood based on the composite fermion (CF) model [1], where basic particles are CFs obtained by attaching an even number of flux quanta to electrons. At the filling factor $\nu = 1/2$, the attached flux exactly cancels the applied magnetic field, giving rise to a Fermi liquid state of CFs [2]. As the field deviates from $\nu = 1/2$, CFs are subjected to an effective magnetic field $B^* = B - B_{1/2}$, by which the series of FQHE at $\nu = p/(2p \pm 1)$ can be interpreted as the integer QH effect (IQHE) of CFs at $\nu_{\mathrm{CF}} = p$. The noninteracting CF model has been successfully used to interpret the activation gaps [3] and spin-polarization transitions [4,5] in various FQHE states, and the cyclotron resonance of CFs [6]. Consequently, the interactions between CFs, which underlie these phenomena and the existence of CF per se, are incorporated in the effective mass of CFs defined for each context [5,7] and do not manifest themselves.

In bilayer systems, the interplay of interlayer and intralayer Coulomb interactions has provided a vast field of many-body phenomena which have no counterpart in individual two-dimensional systems. This is best illustrated in the bilayer QH state at the total filling factor $\nu = 1$ [8], where each layer has a fractional filling of 1/2. The spectacular transition from a strongly correlated incompressible state at lower densities to an uncorrelated or weakly correlated compressible state at higher densities cannot be fully understood within one picture. The system is best described as an easy-plane pseudospin ferromagnet for strong interlayer correlations, while in the other limit of strong intralayer correlations it is better described as two Fermi liquids of CFs weakly interacting with each other. Hence, the FQHE in a bilayer system, in which the interplay of interlayer and intralayer interactions *between CFs* determines the ground state, is a touchstone for noninteracting CF model, and could be a laboratory for studying the underlying interactions.

In this Letter, we study the phase diagram of CFs in the presence of both spin and layer degrees of freedom in the bilayer $\nu = 2/3$ state. The interlayer/intralayer interactions and tunneling energy are controlled through the total electron density $n_t = n_f + n_b$ and the density difference between two layers $\sigma = (n_f - n_b)/n_t$ [9], where n_f (n_b) is the electron density in the front (back) layer. Activation energy measurements elucidate the existence of three different QH states. We also find two types of hysteresis in the magnetoresistance, one of which is specific to bilayer systems. While the noninteracting CF model provides a qualitative account of the phase diagram, the observed renormalization of tunneling gap, Δ_{SAS}, cannot be explained in the noninteracting model, and is a signature of interactions between CFs.

Our sample consists of two 200-Å-thick GaAs quantum wells separated by a 31-Å-thick $Al_{0.33}Ga_{0.67}As$ barrier with $\Delta_{\mathrm{SAS}} = 10.9$ K. The electron density in each layer is controlled by the front and back gate voltages. The low temperature mobility is 2×10^6 cm^2/Vs with $n_t = 2 \times 10^{11}$ cm^{-2}. The sample is mounted on a goniometer with a superconducting stepper motor in a dilution refrigerator operating at 50 mK. Magnetoresistance measurements are performed using a standard low-frequency ac lock-in technique with a magnetic-field sweep rate of 0.06 T/min and a current of 20 nA.

Figure 1 shows the noninteracting CF energy levels in a bilayer system. With the pseudospin language, the energy gap between the bonding (b) and antibonding (a) states, $\Delta_{\mathrm{BAB}} = \Delta_{\mathrm{SAS}}/(1 - \sigma^2)^{1/2}$, is treated as a pseudo-Zeeman energy, which equals Δ_{SAS} at $\sigma = 0$ and increases with applying a bias voltage [10]. The CF-cyclotron energy, which is determined by the perpendicular magnetic field $B_\perp$, can be written as $\Delta_{\mathrm{cy}} = C(\sigma)e^2/4\pi\epsilon l_B^* \propto \sqrt{B_\perp}$ [2], where $C(\sigma)$ is a dimensionless coefficient, ϵ is the dielectric constant, and l_B^* is the magnetic length in B^*. We allow $C(\sigma)$ to be a function of σ to include the finite width of the wave functions. The levels are further split by the Zeeman energy, $\Delta_Z = g^* \mu_B B_{\mathrm{tot}}$, where g^* is the gyromagnetic ratio, μ_B is the Bohr magneton, and B_{tot} is the total magnetic field. We label each CF energy level as

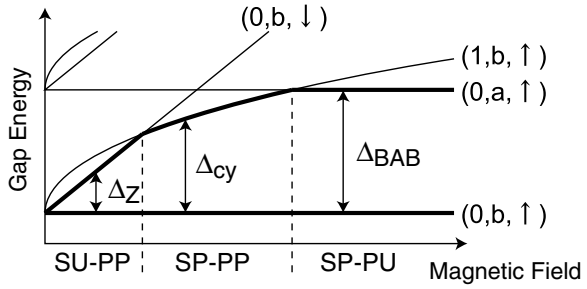

FIG. 1. Lower-lying energy levels of noninteracting CFs schematically shown as a function of the magnetic field. While pseudo-Zeeman energy Δ_{BAB} is constant, the Zeeman $\Delta_Z \propto B_{\mathrm{tot}}$ and CF-cyclotron $\Delta_{\mathrm{cy}} \propto \sqrt{B_\perp}$ energies depend on the magnetic field. At $\nu = 2/3$, the lowest two levels are filled (thick curves), and there are three possible QH ground states. Here, SU-PP means the spin-unpolarized pseudospin-polarized state. $(0, b, \uparrow)$ represents the $N_{\mathrm{CF}} = 0$ Landau level in the bonding state with up-spin.

(N_{CF}, ps, s), where N_{CF} $(= 0, 1)$, ps $(= b, a)$ and s $(=\uparrow, \downarrow)$ are the CF-Landau orbit, pseudospin, and spin indices.

In Fig. 2, we show the evolution of the $\nu = 2/3$ state with n_t in a perpendicular field for two limiting cases, i.e., the balanced-density point ($\sigma = 0$) and the monolayer point ($\sigma = 1$). For both $\sigma = 0$ and 1, the QH state is well developed at high densities, where the magnetoresistance R_{xx} falls to zero. At $\sigma = 0$, the R_{xx} minimum gets weaker with decreasing n_t, and collapses at $n_t = 0.8 \times 10^{11}$ cm^{-2}, followed by a reappearance at $n_t = 0.6 \times 10^{11}$ cm^{-2} [11]. At $\sigma = 1$, a significantly different behavior is observed: R_{xx} shows a hysteresis between upward and downward magnetic-field sweeps in a wide density range, $0.8 \leq n_t \leq 1.2 \times 10^{11}$ cm^{-2}, until it disappears for $n_t = 0.6 \times 10^{11}$ cm^{-2} [12]. We refer to this hysteresis as type G (G stands for the ground state, as we explain later).

We have repeated similar measurements for $0 \leq \sigma \leq 1$ and $0.5 \leq n_t \leq 1.8 \times 10^{11}$ cm^{-2}, and made a phase diagram (Fig. 3). Four QH areas, labeled I, II, III, and IV, are clearly recognized. The diagram reveals that the high-density phase at $\sigma = 0$ (I) exists only at $\sigma = 0$, while the low-density phase at $\sigma = 0$ (II) evolves continuously to the high-density phase at $\sigma = 1$ (III). It is worth noting that, between these regions, there is a non-QH region, which spreads over a wide range of n_t and σ. Type-G hysteresis, observed at $\sigma = 1$ between III and IV, persists for $\sigma < 1$, shifting toward lower n_t with decreasing σ. We also find another type of hysteresis, in a region between II and III (small white squares). We call this type E (E stands for excitation levels) and discuss it later.

The four QH regions in the phase diagram can be identified with the CF energy level diagram shown in Fig. 1. In area I, where n_t is high and σ is small, the large Δ_Z and small Δ_{BAB} lead to the spin-polarized pseudospin-unpolarized (SP-PU) state. In area IV, where n_t is small and σ is large, the small Δ_Z and large Δ_{BAB} result in the spin-unpolarized pseudospin-polarized (SU-PP) state. The spin-polarized pseudospin-polarized (SP-PP) state appears in the intermediate areas (II and III).

The above assignments are confirmed by activation energy measurements with the sample tilted in a magnetic

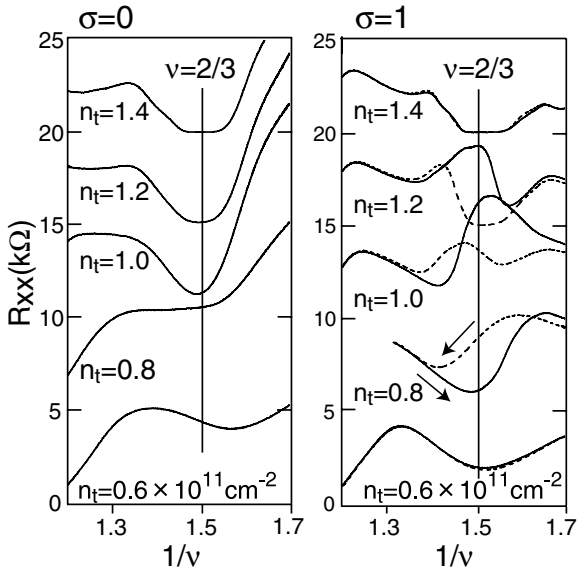

FIG. 2. R_{xx} at the balanced-density point ($\sigma = 0$) and the monolayer point ($\sigma = 1$) for several total densities, plotted as a function of $1/\nu = eB_\perp/hn_t$. Each trace is vertically offset by 5 kΩ. Hysteresis between the upward (solid trace) and downward (dashed trace) field sweeps is seen at $\sigma = 1$.

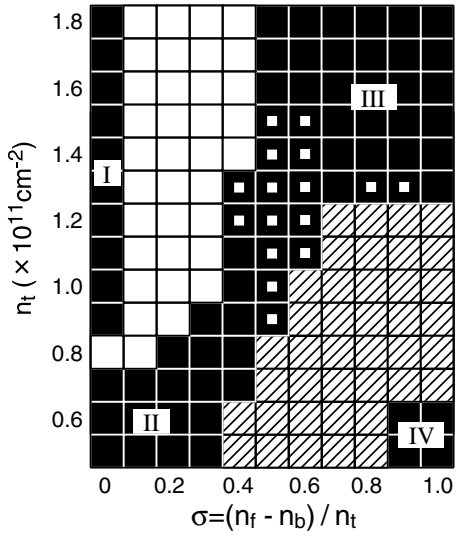

FIG. 3. Phase diagram for $\nu = 2/3$. The horizontal and vertical axes are the normalized density difference between two layers, σ, and the total electron density, n_t, respectively. The black and white areas represent QH and non-QH states, respectively. Type-G hysteresis (Fig. 2) was observed in the hatched area. The small white square in black region indicates the occurrence of a different type of hysteresis (Fig. 5).

field while keeping $B_\perp$ fixed. Figure 4 shows the activation energy, Δ, in the four QH areas as a function of the total magnetic field $B_{\rm tot} = (B_\perp^2 + B_\parallel^2)^{1/2}$, where $B_\parallel$ is the in-plane field. In areas I and III, Δ initially increases with a slope $\partial\Delta/\partial B_{\rm tot} \approx g^*\mu_B$, indicating that the gap is due to spin-reversed excitations from a spin-polarized ground state, consistent with SP-PU (I) and SP-PP (III). Likewise, the spin-polarization transition [14,15] in area IV, seen as the turnover of Δ at $B_{\rm tot} = 5$ T, shows that the ground state is spin-unpolarized for $B_\parallel = 0$, consistent with SU-PP. In area II, an addition of $B_{\rm tot}$ as small as 0.1 T results in a collapse of the gap. This shows that the gap is associated with $\Delta_{\rm BAB}$, which decreases as $\Delta_{\rm BAB} \propto \exp\{-(B_\parallel d/2B_\perp l_B^*)^2\}$ [16] (d is the layer separation) for $\sigma = 0$, consistent with the state being pseudospin-polarized (SP-PP).

Now we examine quantitatively the validity of the non-interacting CF model in bilayer systems. The transition between SP-PP (III) and SU-PP (IV), which is associated with the spin and CF-Landau orbit degrees of freedom, occurs when Δ_Z and $\Delta_{\rm cy}$ become equal [4],

$$g^*\mu_B B_{\rm tot} = C(\sigma)e^2/4\pi\epsilon l_B^*. \quad (1)$$

The observed transition point of $n_t = 0.95 \times 10^{11}$ cm^{-2} for $\sigma = 1$ yields $C(1) = 0.026$. We arrive at a similar value, $C(1) = 0.027$, from the tilted-field data for area IV in Fig. 4. As σ is decreased, we expect $C(\sigma)$ to decrease because electrons tend to extend over both layers, making Coulomb interactions weaker. It follows from Eq. (1) that $B_\perp \propto C(\sigma)^2$ at $\theta = 0$. Indeed, we get $C(0.6) = 0.019$ at the lowest $n_t = 0.5 \times 10^{11}$ cm^{-2}. Hence, n_t at the transition decreases as $n_t = \nu eB_\perp/h \propto C(\sigma)^2$ [17]. This explains why the boundary between SP-PP (III) and SU-PP (IV) shifts toward lower n_t with decreasing σ.

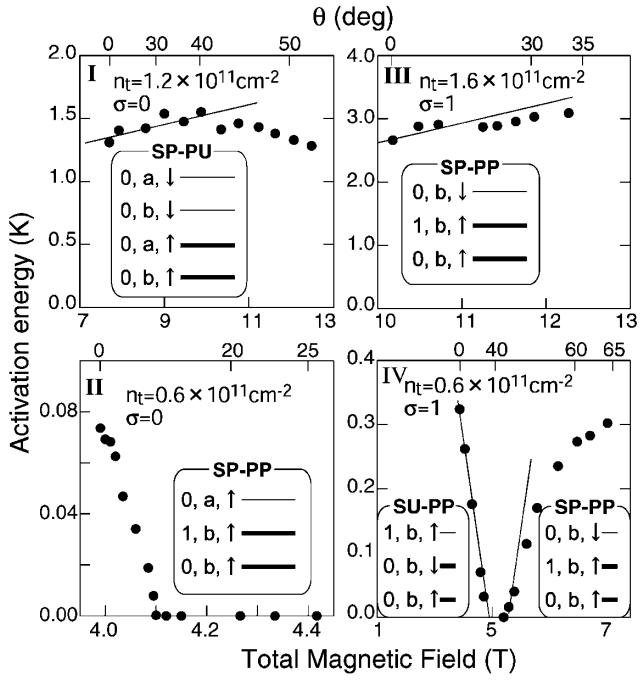

FIG. 4. The activation energy Δ as a function of $B_{\rm tot}$ at $\nu = 2/3$ in the four QH areas. Δ is determined from the temperature dependence, $R_{xx} \propto \exp(-\Delta/2T)$ [13]. On the top axis, we show the tilt angle θ. The leftmost point corresponds to $\theta = 0$ where $B_{\rm tot} = B_\perp$. The slope of the lines included in I, III, and IV correspond to $\pm g^*\mu_B B_{\rm tot}$. In the insets, we showed the ground state of the QH states (thick line) and excitation levels (thin line).

We then proceed to the pseudospin transition between SP-PP (II) and SP-PU (I) at $\sigma = 0$. The noninteracting model predicts that it occurs when $\Delta_{\rm cy}$ equals $\Delta_{\rm BAB}$,

$$\Delta_{\rm BAB} = C(\sigma)e^2/4\pi\epsilon l_B^*. \quad (2)$$

Equation (2) together with the observed transition point of $n_t = 0.8 \times 10^{11}$ cm^{-2} and $\Delta_{\rm SAS} = 10.9$ K gives $C(\sigma = 0) = 0.17$, which is at least 8.9 times larger than the one estimated from Eq. (1). This inconsistency arises partly because the exchange interaction between CFs enhances the Zeeman energy in Eq. (1) [18]. This results in the underestimation of the prefactor C when one uses the bare Zeeman energy as usually done [4,5]. However, the exchange enhancement of the Zeeman energy reported in Ref. [18] is only by a factor of 2.5, so there still remains inconsistency by a factor of $\sim$4. This means that in bilayer systems the interplay of interlayer/intralayer correlations cannot be fully accommodated in a single effective mass of noninteracting CFs and, within the noninteracting CF model, $\Delta_{\rm SAS}$ must be renormalized.

Since the SP-PP and SP-PU states have the same spin polarizations and similar density profiles at $\sigma = 0$, the observed renormalization of $\Delta_{\rm SAS}$ cannot be explained in a simple mean-field picture, which predicts the two states to have similar exchange energies [19]. This, in turn, indicates that the exchange energy in the fractional regime strongly depends on the details of the electronic states. Our results show that the SP-PU state, in which electrons in each layer configure the monolayer $\nu = 1/3$ QH state, has a lower exchange energy than the SP-PP state, making $\Delta_{\rm SAS}$ effectively smaller.

A similar argument has been used to account for the reduction of $\Delta_{\rm SAS}$ and the collapse of the bilayer $\nu = 1$ QH state at high densities [20,21]. The mixing of antibonding states into the many-body ground state allows electrons in the same layer to be more strongly correlated than those in different layers [22,23]. At high densities, where intralayer interactions become dominant, electrons choose to occupy the antibonding state at the cost of tunneling and interlayer correlation energies. While this leads to the softening of charge density excitations and collapse of the QH effect for $\nu = 1$, the same mechanism leads to the transition from the SP-PP to SP-PU state for $\nu = 2/3$.

The same scenario can be applied to the non-QH state spreading for $\sigma > 0$ at high n_t. Note that the SP-PU state is pseudospin-unpolarized and can exist only at the balanced point ($\sigma = 0$). For unbalanced points ($\sigma > 0$), quasiparticles with opposite charges are introduced in different

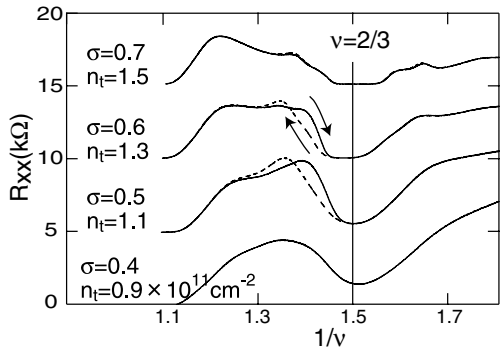

FIG. 5. The evolution of R_{xx} from areas II to III. At $\sigma = 0.5$ and 0.6, type-E hysteresis is seen.

layers, destroying the SP-PU state. Since the non-QH state also has antibonding states occupied, it is expected to have higher intralayer correlations than the SP-PP state. Therefore, the non-QH state persists until the tunneling energy Δ_{BAB} overcomes the intralayer correlation for even larger σ and the SP-PP state becomes lower in energy.

Finally, we discuss the two types of hysteresis. Type G, which is caused by the domain formation at the coexistence of ground states with different spin polarizations [24,25] and the resultant nuclear polarization [26–28], is already known in monolayer systems. Type E is distinguished by the observation that R_{xx} for both upward and downward field sweeps takes a well-developed minimum at $\nu = 2/3$ (Fig. 5), meaning that there is no degeneracy in the $\nu = 2/3$ ground state. This observation, combined with the fact that type G vanishes already at $n_t = 1.3 \times 10^{11}$ cm^{-2} for $\sigma = 1$ and moves further away toward lower B for smaller σ (Fig. 3), clearly indicates that the hysteresis in Fig. 5 has a different origin. As the data in Fig. 4 show, the excitation level of the SP-PP state changes from $(0, b, \downarrow)$ in area III to $(0, a, \uparrow)$ in area II due to the reduction in Δ_{BAB} with decreasing σ. Hence, in the intermediate region, these excitation levels become degenerate, allowing for two types of quasiparticles in the flanks of $\nu = 2/3$. Hysteresis can arise because the energies of these quasiparticles, having opposite spins, depend on the Zeeman energy and hence the hyperfine field from the nuclei. At $\nu = 2/3$, the SP-PP state, having no competing ground state, develops independent of the hyperfine field. Our observations indicate that the FQHE ground state degeneracy is not a prerequisite for hysteretic behavior. Rather, coincidence of any CF levels with opposite spin at the Fermi energy can open the spin-flip channel with nuclear spins.

In summary, we have studied the phase diagram of bilayer $\nu = 2/3$ and identified three different QH ground states and two types of hysteresis. While the noninteracting CF model provides a qualitative account of the phase diagram, the observed renormalization of tunneling gap, Δ_{SAS}, indicates that the exchange interactions between CFs are nontrivial.

The research was supported in part by Grants-in-Aid for the Scientific Research from the Ministry of Education, Science, Sports and Culture (No. 10203201, No. 11304019, No. 08159), the Mitsubishi Foundation, and the Asahi Glass Foundation, CREST-JST and NEDO "NTDP-98" projects.

[1] J. K. Jain, Phys. Rev. Lett. **63**, 199 (1989).
[2] B. I. Halperin, P. A. Lee, and N. Read, Phys. Rev. B **47**, 7312 (1993).
[3] R. R. Du *et al.*, Phys. Rev. Lett. **70**, 2944 (1993).
[4] R. R. Du *et al.*, Phys. Rev. Lett. **75**, 3926 (1995).
[5] I. V. Kukushkin, K. v. Klitzing, and K. Eberl, Phys. Rev. Lett. **82**, 3665 (1999).
[6] I. V. Kukushkin *et al.*, Nature (London) **415**, 409 (2002).
[7] K. Park and J. K. Jain, Phys. Rev. Lett. **80**, 4237 (1998).
[8] S. Q. Murphy *et al.*, Phys. Rev. Lett. **72**, 728 (1994).
[9] A. Sawada *et al.*, Phys. Rev. Lett. **80**, 4534 (1998).
[10] K. Muraki *et al.*, Solid State Commun. **112**, 625 (1999).
[11] T. S. Lay *et al.*, Phys. Rev. B **56**, R7092 (1997).
[12] Although the width of the hysteresis depends on the field sweep rate and the current, the conditions used are suitable to judge the existence or absence of the hysteresis.
[13] Some gaps are in the order of 10 mK, which is the same order of the experimental temperature. We have confirmed that qualitatively the same results are obtained from the Liftshitz-Kosevich formula valid also for small energy gaps [D. R. Leadley *et al.*, Phys. Rev. Lett. **79**, 4246 (1997)].
[14] J. P. Eisenstein *et al.*, Phys. Rev. B **41**, 7910 (1990).
[15] L. W. Engel *et al.*, Phys. Rev. B **45**, 3418 (1992).
[16] J. Hu and A. H. MacDonald, Phys. Rev. B **46**, 12 554 (1992).
[17] Although the SU-PP is expected to extend toward $\sigma = 0$ for lower n_t, the observation of the FQHE for $n_t \leq 0.4 \times 10^{11}$ cm^{-2} is hampered by the reduced mobility.
[18] I. V. Kukushkin *et al.*, Phys. Rev. Lett. **85**, 3688 (2000).
[19] This contrasts with the phase transition in bilayer $\nu = 2$ [9], which can be understood in a mean-field picture as a spin-unpolarized to polarized transition driven by the intralayer/interlayer exchange energy.
[20] G. S. Boebinger *et al.*, Phys. Rev. Lett. **64**, 1793 (1990).
[21] Since the SP-PP state is a hole analog of $\nu = 1/3$ in the monolayer ($\sigma = 1$) and large Δ_Z limit, it is tempting to consider the SP-PP state for $0 \leq \sigma < 1$ as a CF analog of bilayer $\nu = 1$. The collapse of the SP-PP state upon applying a small $B_{\|}$ seems to be consistent with this idea [8]. This, however, requires further investigations.
[22] A. H. MacDonald, P. M. Platzman, and G. S. Boebinger, Phys. Rev. Lett. **65**, 775 (1990).
[23] L. Brey, Phys. Rev. Lett. **65**, 903 (1990).
[24] J. Eom *et al.*, Science **289**, 2320 (2000).
[25] J. H. Smet *et al.*, Phys. Rev. Lett. **86**, 2412 (2001).
[26] S. Kronmüller *et al.*, Phys. Rev. Lett. **81**, 2526 (1998).
[27] J. H. Smet *et al.*, Nature (London) **415**, 281 (2002).
[28] K. Hashimoto *et al.*, Phys. Rev. Lett. **88**, 176601 (2002).